J Nondestruct Eval (2017) 36:70
https://doi.org/10.1007/s10921-017-0451-3

Simulation of Laser Ultrasonics for Detection of Surface-Connected Rail Defects

Zhong Yunjie[1] · **Gao Xiaorong**[1] · **Luo Lin**[1] · **Pan Yongdong**[2] · **Qiu Chunrong**[1]

Received: 12 November 2016 / Accepted: 21 September 2017 / Published online: 26 September 2017

Abstract Laser ultrasonic produces frequencies in the MHz range, enabling high accuracy and a strong ability to detect rail surface defects. This paper mainly studied on the simulation of detecting surface-connected rail defects on 60 kg rails with laser ultrasonic, established the finite element model of laser-excited ultrasonic Rayleigh wave, carried out the simulation, and verified the effectiveness of the technology through experiments. To solve the problem that laser ultrasonic is insensitive to the width of defects in actual detection, and unable to make quantitative detection of defects, this paper established a new model on the basis of improving the original model that has been verified, exciting ultrasonic at the two sides at the same time of a rail with two staggered beams of laser separately to detect irregular scratch defects on rail surface, and two groups of signal data were received through two probes. Each group of data can present the half-profile information of defects, and further form two detection images of the defect. At last, the two detection images were combined into a complete image through image processing. The results of the experiment indicate that the technology studied offers a new method for the effective quantitative detection of surface-connected defects on rail.

Keywords Laser ultrasonic · Surface-connected rail defects · Finite element method · Image processing

✉ Zhong Yunjie
yunjie_zhong@163.com

[1] School of Physical and Technology, Southwest Jiaotong University, Chengdu 610031, China

[2] School of Aerospace Engineering and Applied Mechanics, Tongji University, Shanghai 200092, China

1 Introduction

The ultrasonic technology finds wide applications in the non-destructive testing of rail surface defects [1]. In the conventional ultrasonic technology, a short pulse wave is sent and received through the same transducer to detect defects, the ultrasonic wave usually is of the single mode at low frequency, thus being unable to realize the highly sensitive and all-round detection [2–4]. The laser ultrasonic technology can excite the ultrasonic wave of multiple modes in a detected object, and the frequency can reach MHz range. It cannot be replaced by conventional ultrasonic in the non-destructive testing of tiny defects [5,6]. The high accuracy requirement in rail surface defects detection, so the study of detecting rail surface defects with the laser ultrasonic technology is of the great application value.

Ultrasonic wave propagation can be studied analytically by solving the governing equations of motion together with the related boundary conditions in theory. Sanderson [7] solved heat conduction and thermal-elastic equation through the eigenfunction expansion method, but the method was applicable to the analysis of very thin materials. With regard to samples of the given thickness, high-frequency component of lower-order mode and higher-order mode should be taken into consideration, thus resulting in computing complexity. When conducting analytical algorithm through Green function method, Rose [8] used the point-source model but ignored that heat penetration effect of laser action became surface heat source. As for the actual Gaussian pulse 2D model, Bresse et al. [9] made use of Laplace-Hankel transformation method to solve the heat conduction equation easily, but it was difficult to re-transform solutions into the time-space coordinate system through the analytical method in general cases. Therefore, numerical methods are needed for the better theoretical study of laser ultrasonic problems. Basic

numerical methods include boundary element method and finite element method. With some limitations, the former is applicable to the model that sample surface should be discretized, and the latter is usually used as a better tool for the study of laser ultrasonic [10,11]. Finite element can be employed to flexibly handle complicated geometrical models, and even anisotropic materials [12]. In 1985, Kasai [13] analyzed the ultrasonic signal with the laser-excited frequency being below 100 KHz in single-layer copper materials through the finite element method. In 1995, Lee [14] brought forth the finite element model of laser Lamb wave, and numerically simulated the waves of lower-order mode with analytical solutions. In 2001, Wu [15] simulated the excitation process of surface wave in cylinders through finite element method. In 2003, Hassan [16] through finite element modeling, exposed the relationship between ultrasonic reflection coefficient and transmission coefficient and defect characteristics after the defect effect of surface acoustic wave, thus creating the theoretical foundation for the quantitative identification of surface defects. And in 2011, Edward [17] studied the realistic model of inclination angle defects, such as rolling contact of rails, simulated ultrasonic signals generated from different defect angles through finite element, considered the impact of defect shapes, and explained the reasons for the enhancement of detection signal close to defects.

The paper established the numerical model of rail surface defects with laser-excited ultrasonic verified the correctness of the model through the experimental method, and presented a new model through improving the verified model. The new model offers a new method for the effective and quantitative detection of tiny defects on rail surface. The structure of the paper is as follows: Part II describes the principle of laser-excited ultrasonic, and sets up the finite element model of detecting rail surface-connected defects with laser ultrasonic; Part III verifies the correctness of the model and the effectiveness of defect detection through the experimental method, and proves that the new model can effectively and quantitatively detect irregular scratch defects on rail surface; and Part IV is the conclusion of the paper.

2 Theory

2.1 Laser-Excited Ultrasonic Theory

Exciting ultrasonic wave on material surface by laser is a multi-physical field coupling process. High-energy laser beams are radiated on the surface of materials, and part of the luminous energy is absorbed by materials and converted into thermal energy, thus causing local temperature changes. Due to thermal expansion, there forms the elastic stress wave in materials, namely ultrasonic wave. The current mechanisms of laser excitation include thermal-elastic mechanism, ablation mechanism, medium damage theory, electrostrictive and magnetostrictive theories, and gasification expansion mechanism. In ordinary materials, electrostrictive or magnetostrictive deformation caused by light is rather minor, and gasification expansion process can hardly be controlled. The study of the medium damage mechanism remains in the experimental stage. Comparatively speaking, thermal-elastic mechanism and ablation mechanism are perfect, and described with the complete mathematical model. Under thermal-elastic mechanism, the intensity of laser beams radiated on material surface is low, and the optical power density of laser is inadequate for melting material surface. Therefore, some energy of laser is absorbed by the shallow surface of materials, and some reflected by the surface. The temperature of the shallow surface of materials rises quickly due to the absorption of laser energy, and at the same time, internal kinetic energy of crystal lattice is on the rise as well. Within the elastic limit, thermo-elastic expansion caused by the rise of temperature further leads to deformation. Since the incident laser is pulse laser, so the thermo-elastic expansion is periodic, namely generating periodic pulsed ultrasonic wave. Under the ablation mechanism, the incident laser power density is higher than the damage threshold of material surface, so material surface is melted and gasified to form plasma, which quickly leaves from material surface to generate a kind of acting force vertical with material surface, and further generate the stress wave.

2.2 Modeling

The finite element method can be used to solve the multi-physical field coupling problem conveniently, and produce the numerical solution of the whole field, so it is applicable to studying sound field computing of laser ultrasonic. Thermal-elastic excitation mechanism refers to the fact that laser radiation causes local temperature change of material surface, and ultrasonic wave is thus excited by the effect of thermal expansion. Thermal-elastic coupling control equation for surface wave excited by laser is:

$$\begin{cases} K\nabla^2 T = \rho c_v \dot{T} + \beta T_0 \nabla \cdot \dot{U} - Q \\ \mu\nabla^2 U + (\lambda + \mu)\,\nabla(\nabla \cdot U) = \rho\ddot{U} + \beta\nabla T \end{cases} \tag{1}$$

where K, ρ and c_v are materials' thermal conduction coefficient, density, and specific heat capacity under stable deformation respectively; T and T_0 are transient temperature and environmental temperature respectively; U is transient displacement vector; λ and μ are Lame coefficients; β is thermal-elastic coupling coefficient of materials, $\beta = (3\lambda + 2\mu)\,\alpha$, and α is the coefficient of thermal expansion of materials. $\beta\nabla T$ is the impact of temperature field on ultrasonic field. $\beta T_0 \nabla \cdot \dot{U}$ is related to the stress of materials at each point. The value indicates the impact of ultrasonic

field on temperature field. When the value is positive, its effect is contrary to that of heat source Q. The temperature declines due to the "absorption of heat". Therefore, when laser excites ultrasonic wave on material surface, ultrasonic field also affects temperature field, and the complete coupling method should be adopted accordingly.

The space and time distributions of laser energy are approximate to Gaussian distribution function, and can be indicated with $g(t)$ and $f(r)$ respectively:

$$g(t) = \frac{8t^3}{t_0^4} \exp\left(-\frac{2t^2}{t_0^2}\right) \tag{2}$$

$$f(r) = \frac{2}{R_G\sqrt{2\pi}} \exp\left(-\frac{2(r-r_G)^2}{R_G^2}\right) \tag{3}$$

where t_0 is the rising time of laser, R_G half width of laser, and r_G coordinate of laser center. Thermal current energy generated on material surface by laser radiation can be described as:

$$Q = E_0 A f(r - r_0)\, g(t) \tag{4}$$

where E_0 is the energy on per unit length of laser, A the absorption rate of material surface, and Q the total energy absorbed by material surface. When the energy of laser radiation is absorbed by materials, local temperature of material surface will rise. With the continuous transmission of the energy absorbed to the surrounding area, there will form a transient heterogeneous temperature field. In the whole process, luminous energy is converted into thermal energy, and further into acoustic energy. The conversion of thermal energy from acoustic energy is realized mainly through thermal conduction and thermal expansion, namely that thermal conduction generates gradient temperature field, thus causing thermal expansion, exciting local vibration of materials, and further converting thermal energy into acoustic energy. The rising time of laser is at the level of nanosecond, so the control Eq. (1) can be simplified as:

$$\begin{cases} K\nabla^2 T = \dot{T} - Q \\ \mu\nabla^2 U + (\lambda+\mu)\nabla(\nabla\cdot U) = \rho\ddot{U} + \beta\nabla T \end{cases} \tag{5}$$

Its finite element form can be expressed as:

$$\begin{cases} [S]\{T\} + [C_V]\left\{\dot{T}\right\} = \{Q\} \\ [M]\left\{\ddot{d}\right\} + [C]\left\{\dot{d}\right\} + [K]\{d\} = \{F\} \end{cases} \tag{6}$$

where $[S]$ is the thermal conduction matrix, $[C_V]$ the thermal capacity matrix, and $\{Q\}$ the heat source vector; $\{T\}$ and $\left\{\dot{T}\right\}$ are the node temperature and change rate of node temperature respective; $[M]$ is the mass matrix, $[C]$ the damping matrix, $[K]$ the stiffness matrix, and $\{F\}$ external force vector formed by transient thermal strain; $\left\{\ddot{d}\right\}$ $\left\{\dot{d}\right\}$ and $\{d\}$ are the accelerated speed, speed, and displacement respectively, which can be obtained through the summation of integrals on all units:

$$\{F\} = \sum\nolimits_e \int [B]^T [D]\{\varepsilon_0\}\, dS \tag{7}$$

where $[B]$ is the strain matrix, $[D]$ is the elastic matrix of materials, and $\{\varepsilon_0\}$ is the thermal strain vector. In Eq. (6), different finite element expressions can, in theory, be used to establish its step-by-step integration equation, but the central difference method is more efficient compared with other methods. In the central difference method, speed and accelerated speed can be expressed with displacement:

$$\begin{cases} \left\{\dot{d}\right\}_t = \frac{1}{2\Delta t}\left(\{d\}_{t+\Delta t} - \{d\}_{t-\Delta t}\right) \\ \left\{\ddot{d}\right\}_t = \frac{1}{\Delta t^2}\left(\{d\}_{t+\Delta t} - 2\{d\}_t + \{d\}_{t-\Delta t}\right) \end{cases} \tag{8}$$

Substitute Eq. (8) into Eq. (6):

$$\begin{aligned} &\left[\frac{1}{\Delta t^2}M + \frac{1}{2\Delta t}C\right]\{d\}_{t+\Delta t} \\ &= \{\mathrm{F}\}_t - \left([K] - \frac{2}{\Delta t^2}[M]\right)\{d\}_t \\ &- \left(\frac{1}{\Delta t^2}[M] - \frac{1}{2\Delta t}[C]\right)\{d\}_{t-\Delta t} \end{aligned} \tag{9}$$

Time step and spatial grid size are two key factors that affect the stability of the numerical system and the spatial sampling of wave modes in a time-domain simulation method. For the former time step is essential for the time resolution and stability of a numerical method. If the time step is larger the method loses its stability. Smaller time step requires much computing time. For the spatial sampling of wave modes the spatial grid size is the main parameter. However there is a close connection between spatial and temporal grid.

Usually for a 2D time-domain simulation method, the spatial grid size and time step can be described as:

$$\Delta x = \frac{c_{min}}{20 f_{max}} \tag{10}$$

$$\Delta t = \frac{1}{c_{max} \times \left(\frac{1}{\Delta x^2} + \frac{1}{\Delta y^2}\right)} \tag{11}$$

where f_{max} is the maximum frequency in the excitation signal, c_{min} is the lowest phase velocity and c_{max} the highest group velocity of the model. Δt condition must be strictly fulfilled. If the time step is larger the method loses its stability. Δx condition in contrast is a "weak" condition. If the grid size is larger numerical dispersion will increase but the method remains stable.

3 Results

3.1 Model Verification

ABAQUS software is used for simulation, Young modulus of the 60 kg rail material used is 210GPa, Poisson ratio is 0.29, density is 7840 kg m^{-3}, and thermal expansion coefficient is 1.18×10^{-5} K. Other thermal-physical parameters are shown as Table 1, and these parameters change with the temperature. It is assumed that laser is evenly distributed along the direction of Z axis, and laser source tends to be long infinitely. In the case, the problem of surface wave excited by laser radiation can be simplified and studied with the plane strain model, shown as Fig. 1a. The initial model adopts a beam of laser to excite ultrasonic wave at the right side of railhead, and the central frequency of the ultrasonic wave excited is 5 MHz. Figure 1b is the FEM mesh generation. Laser action region employed 2046 dense grids with size of 0.03 mm. 7920302 wide grids were set in other regions of railhead, the grid size is 0.06 mm. And the area between the two regions mentioned above adopted 7065 uniform transition grids from 0.03 mm to 0.06 mm. Rail web and rail flange adopted the wide grids. The time step of model is 2 ns, and the total time is 60 μs. Typical computation times of the model is 4 hours on an ordinary PC.

To verify the correctness of the laser ultrasonic finite element model, the results of finite element simulation are compared with experimental results. The experimental platform is the laser ultrasonic field detector which was independently developed by Shanghai Tongji University shown as Fig. 2a. The working principle of the detector is that ultrasonic wave is excited on the detected object through laser, and then received by a piezoelectric ultrasonic wave detector, which is a 72° surface wave probe with the frequency being 2.5 MHz. Data was collected and processed through system software which was independently developed by Shanghai Tongji University to produce the visualized result of ultrasonic field. The system is mainly used for the verification of the laser ultrasonic non-destructive testing principle technology and the study of the ultrasonic field visualization method. Fig. 3a and b are the time domain waveforms obtained through finite element simulation and experimental method respectively, and they show that signal of surface acoustic wave can be well detected through both of the two methods, and the waveforms are extremely similar. In the simulation, laser is arranged at the position shown as Fig. 1a, and the detection point at C position. The transmission route of surface wave is 50 mm long in total. Figure 3 reveals that the time of surface wave flight is 17 μs in the simulation, and the simulated speed of ultrasonic surface wave in the 60 kg

Table 1 Thermal-physical parameters of rail material used in finite element simulation

Temperature (K)	25	100	200	300	400	500	600	700	800	900	1000	1100
Specific heat (J kg^{-1} k^{-1})	472	480	498	524	560	615	700	1000	806	637	602	580
Thermal conductivity (W m^{-1} k^{-1})	93.23	87.68	83.53	80.44	78.13	76.02	74.16	71.98	68.66	66.49	65.92	64.02

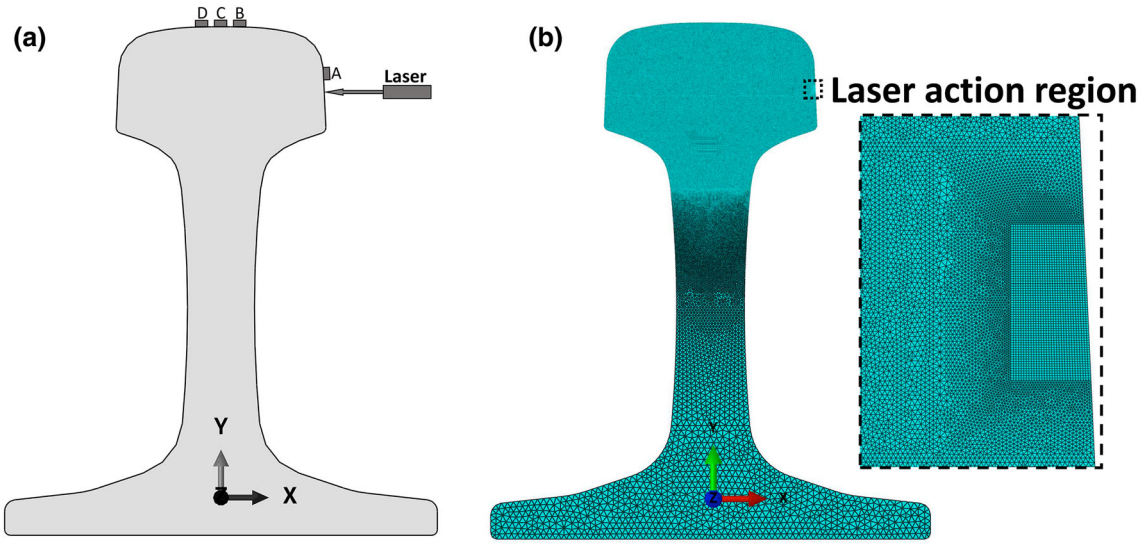

Fig. 1 **a** Equivalent finite element model of defect-free surface of rails radiated by laser. B, C, and D are three different positions, and **b** FEM mesh generation

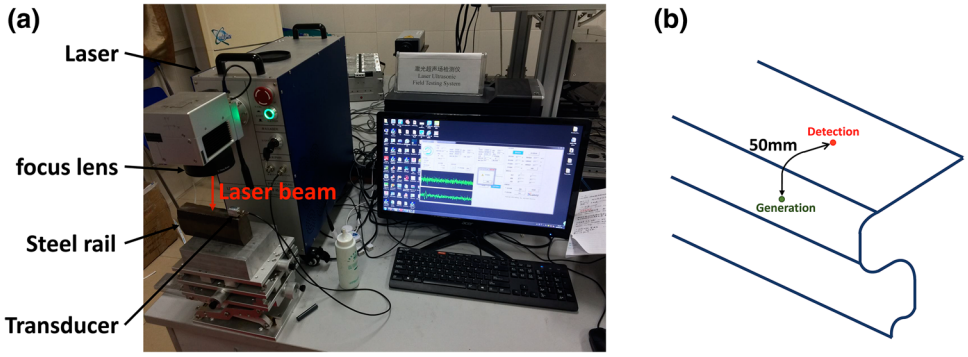

Fig. 2 **a** Is experimental platform for rail detection with laser ultrasonic, and **b** is the generation and detection schematic graph

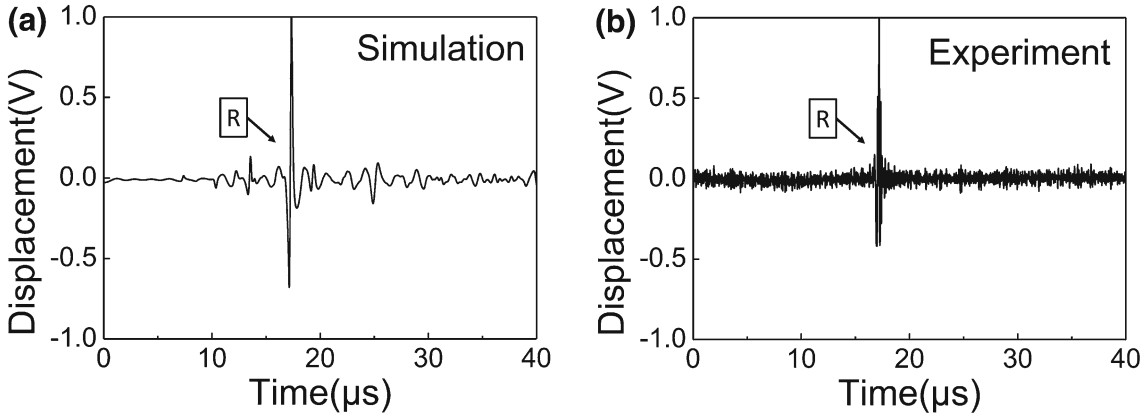

Fig. 3 Speeds of surface waves in the simulation and experiment are compared through the calculation of time-domain signal wave speeds, and R is the Rayleigh wave received. **a** Is the simulation, and **b** is the experiment

rail obtained through computing is 2941.2 m/s. Through the experimental method with the laser ultrasonic field detector, Fig. 2b is the generation and detection schematic graph, the speed value of surface wave in the rail is measured to be 2923 m/s according to the relationship between transmission route and time, and the theoretical speed calculated is 2990 m/s. This shows that the speed obtained in finite element simulation is rather close to the value obtained through the experimental method. It is also discovered in Fig. 3 that their data trends in time domain are very similar as well, thus verifying the correctness of the model.

Rail surface radiated by laser is simulated through the finite element method to produce the distribution of temperature field and stress field of the shallow surface of rails, shown as Fig. 4. It can be discovered that the distribution of temperature field just appears in a small area of rail surface radiated by laser, and there partially forms the corresponding stress field due to thermal expansion.

Figure 5 shows the computing result of temperature field. During and after laser action, there will be no meaningful temperature rise 120 μm away from the laser radiation center along the normal direction N and 150 μm away from the laser radiation center along the radial direction R. This means that the temperature field generated by laser energy absorbed in rail material is concentrated in a very small area, which becomes the body heat source. Ultrasonic wave in materials is the result of the joint effect of surface heat source and body heat source.

Excitation by pulse laser may lead to the partial vibration of materials, and further produce ultrasonic wave. Figure 6 indicates the velocity field of the model at the moment of 3 μs . Since the energy of longitudinal wave generated by laser under the way of thermal-elastic excitation is mainly ranged between 60° and 80°, the energy of shear wave ranged between 30° and 60°, and the energy of surface wave close to 90°. Therefore, the figure of velocity field at the moment of 3 μs can reveal the transmission of waveform of each mode. Figure 7 indicates the A scanning waveform detected at the three points B, C, and D of rail separately, among which surface wave is of double polarities. Apart from surface wave, there are some surface longitudinal waves.

3.2 Detection of Rail Defects

Ultrasonic wave is produced on rail surface through laser radiation, and transmitted along rail surface, shown as Fig. 8. As for rails without surface defects, ultrasonic wave will be transmitted infinitely along the surface; as for rails with surface defects, ultrasonic wave will meet the Huygens prin-

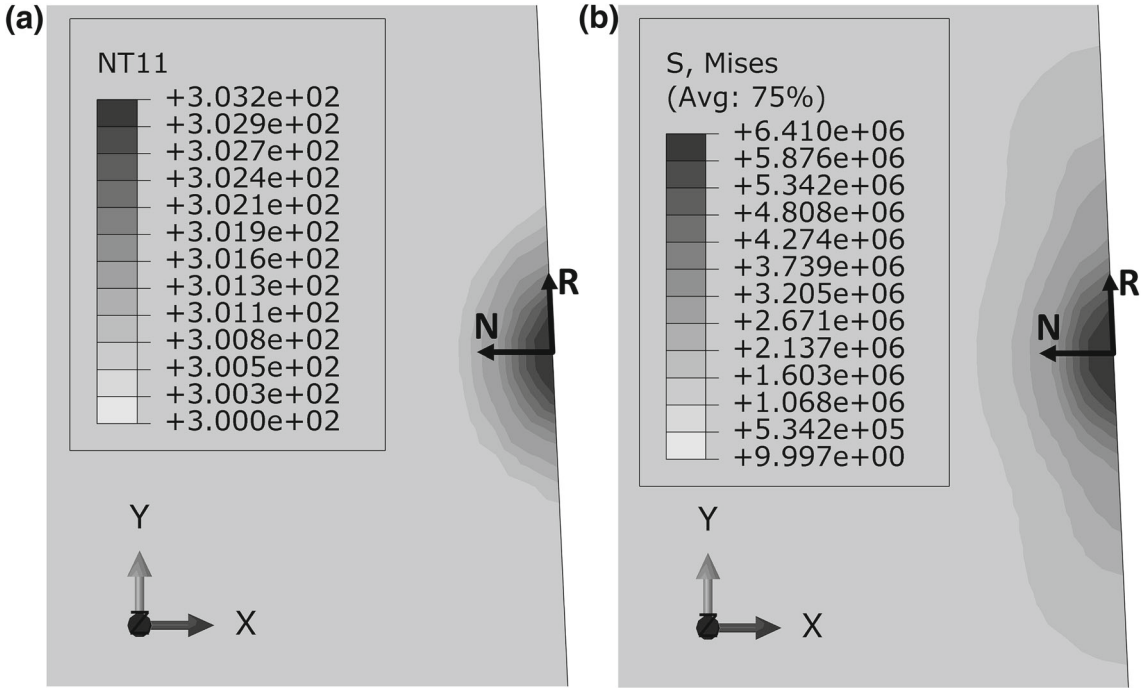

Fig. 4 **a** Indicates the distribution of temperature, and **b** is the distribution of stress field. When laser radiated on rail surface, the fields are distributed in a small area

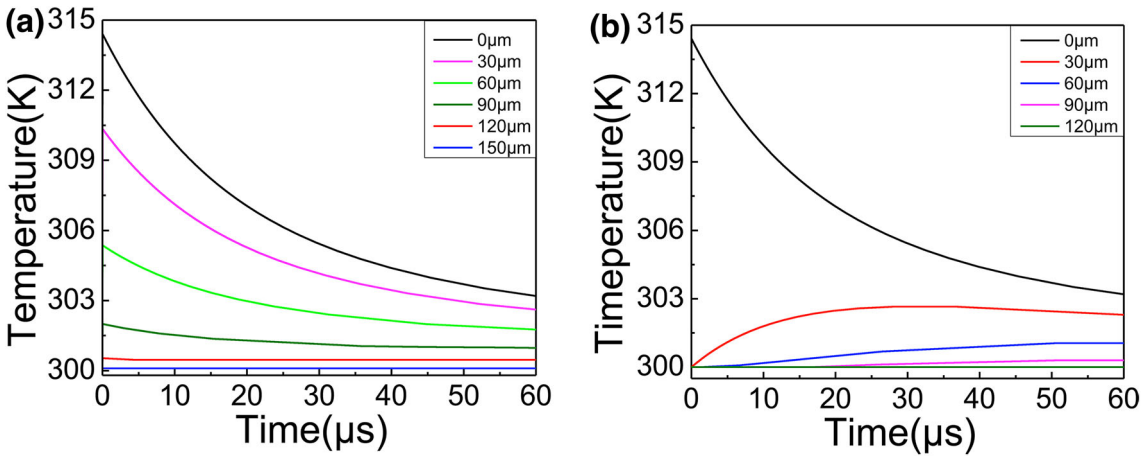

Fig. 5 **a** Indicates the changes of temperature at different radial positions away from the laser excitation point, and **b** indicates the changes at different longitudinal positions

ciple after encountering defects, and be scattered at the points of defects. Part of surface wave is reflected to form reflection echo; part is transmitted continuously after passing through defects; and part is converted into wave of other modes.

In Fig. 1, Point A of the model is taken as the receiving point of surface wave, and defects are arranged at the points of B, C, and D separately, with the size: 0.5 mm × 2 mm. After surface wave is produced by laser and transmitted, the signal received by the detector is displayed as the waveform of Fig. 9. The figure shows that due to the existence of such defects, the detector will definitely detect surface echo at the point of A. In addition, due the different distances from the receiving point to the three defect positions, the time lengths needed for receiving surface echo will be different. The closer the defect is to the receiving point, the less time is needed to detect surface echo. The position information of defects can be obtained precisely according to the relationship between time and speed, and the characteristics of defect signal are especially distinct. Therefore, tiny defects on rail surface can be effectively detected through the laser ultrasonic technology.

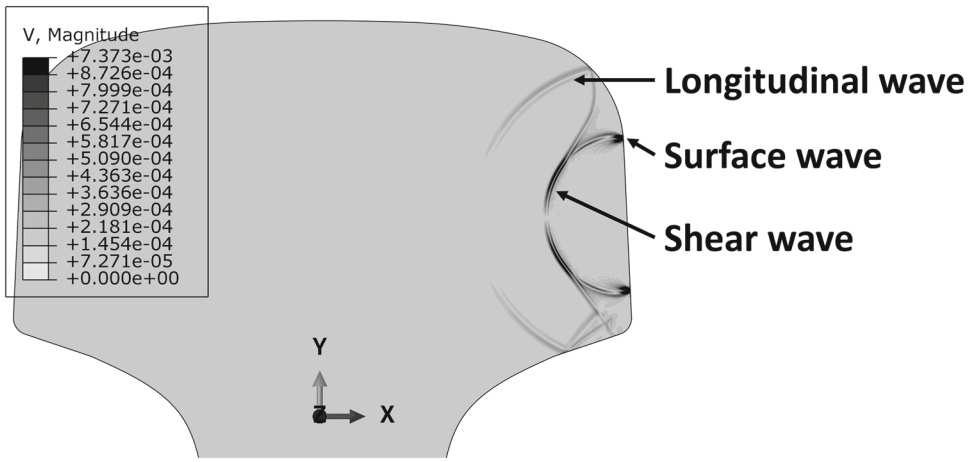

Fig. 6 Velocity field of the model at the moment of 3 μs

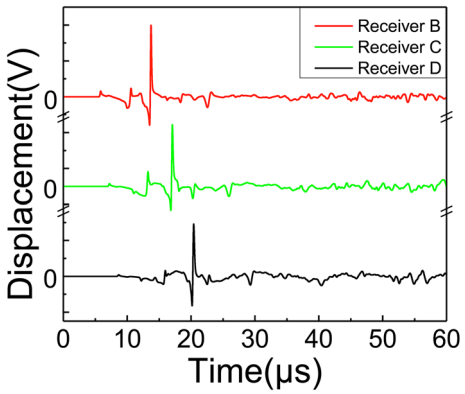

Fig. 7 Time domain signals detected at the three receiver B, C, and D of rail relating to Fig. 1

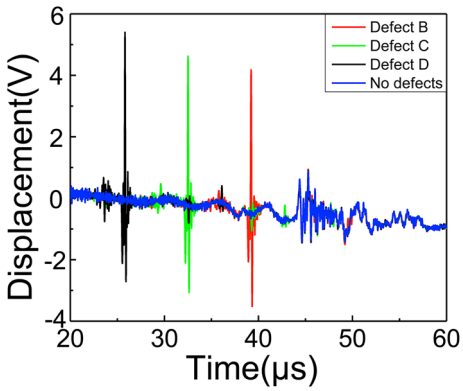

Fig. 9 Comparison of time-domain waveforms obtained at different positions of defects on rail and time-domain waveform obtained from defect -free Rail. Defect size: $0.5\,mm \times 2\,mm$

3.3 Imaging Analysis

After ultrasonic surface wave generated by laser encounters defects, depth information of defects on rail surface can be calculated out. Since surface wave is insensitive to width, it is difficult to make the quantitative analysis of defects. To solve the problem, the paper improves the initial model to some degree, and the improved model uses two beams of laser for staggered excitation at the two sides of railhead. Detection is separately conducted at A point about 5 mm above the

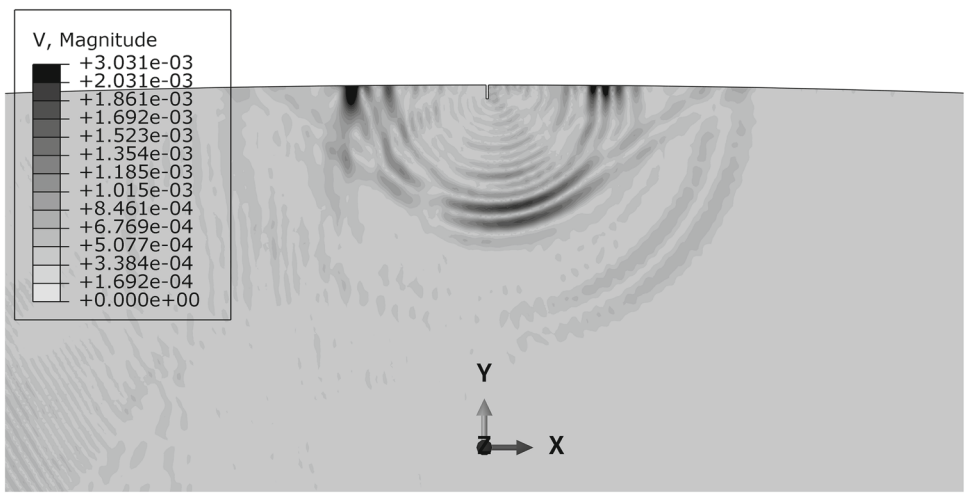

Fig. 8 Sketch map for the scattering of surface wave after encountering defects according to the Huygens principle

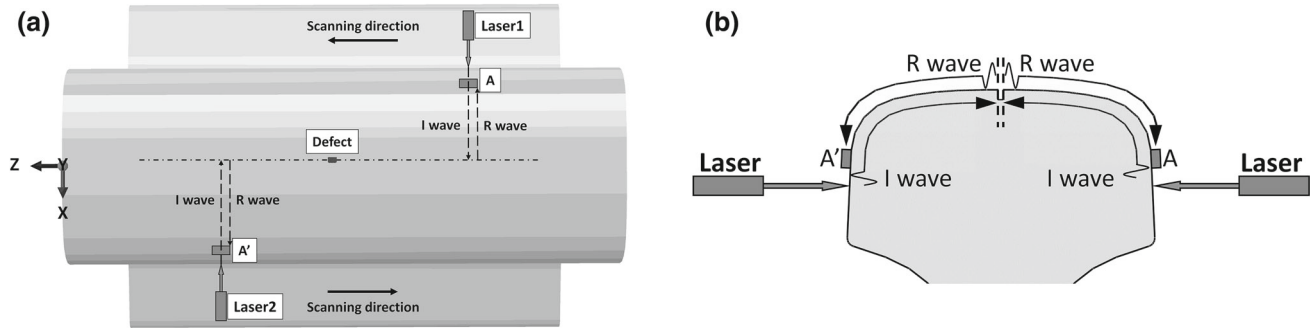

Fig. 10 Improved model, which adopted two lasers to excite ultrasonic and the receivers were set at A and A', **a** Is 3-D view of the model, and **b** Is 2-D view of the model

radiation point and at the position of the other side corresponding with A point. It deserves attention that two lasers are arranged on different planes for staggered excitation, so the transmission route of surface wave is the difference between the distance that is two times that from the exciting point to a defect and the distance from the exciting point to a detecting point, which is indicated as the model of two-point excitation and two-point receiving of Fig. 10. When surface wave encounters defects on rail surface, echo is transmitted to the detectors along the surface.

There is the great deal of friction between wheel set and rail tread, so irregular and tiny scratches often appear on rail tread. Such defects can hardly be detected through ordinary ultrasonic methods, and imaging is the commonly used scratch detection method, according to which rails are imaged for the extraction of abnormal information. However, for the low precision, the method cannot be used for detecting tiny scratch defects. Shown as Fig. 11, such scratch defects are arranged on the surface of rail model, and their shapes are irregular, with the maximum width being 1.75 mm, and depth 0.5 mm. Since $V = f \cdot \lambda$ and the length of surface wave obtained is 1.196 mm, within the range of detection.

At the start of detection, the two lasers not in the same plane excite ultrasonic wave at the two sides of rail, which is transmitted along rail surface. Echo will be generated after surface wave encounters defects. After the data are collected by the corresponding detectors. In the process of detection, the lasers make the scanning along the Z direction of the side of railhead, with the scanning interval being 0.5 mm, and scanning length 20 mm. Two groups of ultrasonic data will be acquired after alternative scanning and data receiving, and each group is the 2D data under multiple domains. According to the relationship between speed and time, time coordinate can be converted into position coordinate, shown as Fig. 12a and b. The profile of defects close to the end of ultrasonic excitation is very clear, and that of defects at the other side is unclear. This means that each group of data can only present half information of defects, which verifies that ultrasonic wave is insensitive to the width of defects.

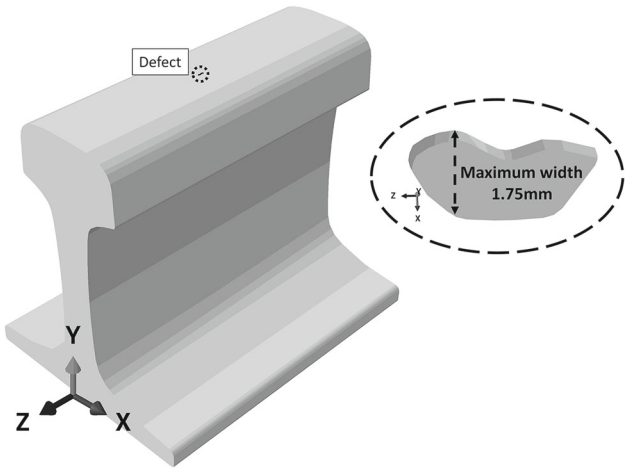

Fig. 11 Sketch map for irregular scratch defects on rail surface, with the depth being 0.5 mm and maximum width being 1.75 mm

However, since each group can present half information of defects, and determine their position and profile, the two groups of data are combined in the paper to produce the complete defects so as to solve the problem that ultrasonic wave is insensitive to defects.

Directly processing and combining the two groups of data collected through the detectors belongs to the image fusion method of data level fusion. When laser is radiated on rail surface, there will form waves of different modes at the same time. In addition, when acoustic waves encounter defects or boundaries, the conversion of wave modes will take place. Therefore, the data collected will bring about a tremendous amount of noise inevitably, which may have negative impact on the quality of profile images of defects. Before data fusion, useful signal of defect information should be extracted to reduce the interference of noise. The simple threshold processing is adopted here. First of all, the edge with significant pixel changes is extracted through the image characteristic extraction technology of Sobel edge detection. The jump among data of the edge is the biggest, and the threshold value is set as half of the average value of edge jumps. Furthermore,

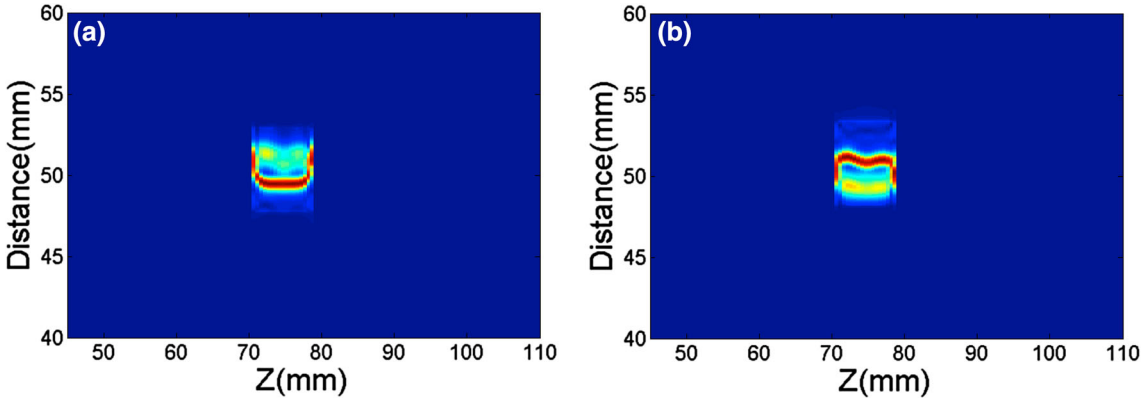

Fig. 12 Results of detecting rail defects with a single laser, **a** is the result of one laser, and **b** is the result of another laser

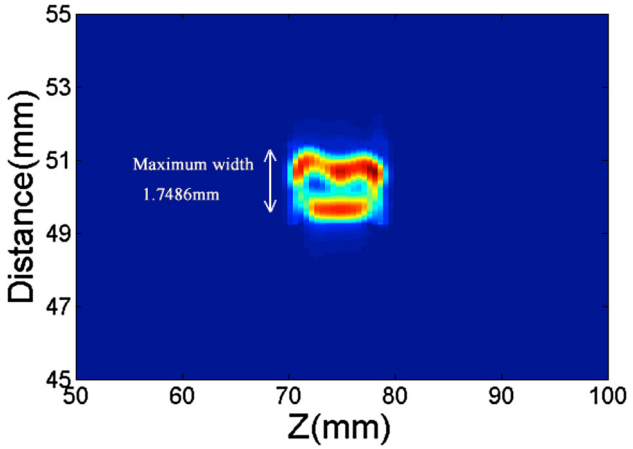

Fig. 13 Imaging result of rail defects after registration (Based on the equal velocity v registration is made according to the difference of time of flight t since route $L = vt$)

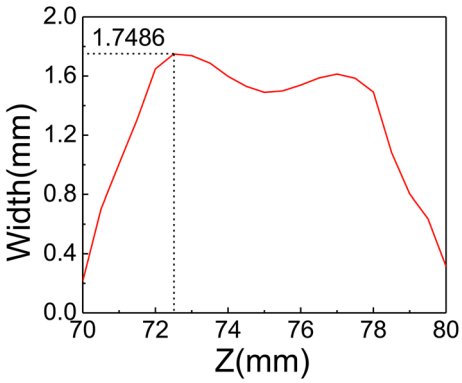

Fig. 14 Defect width change with position Z (Extreme outer edge of defect profile)

only the part with pixels being above the threshold value is preserved. The results shown as Fig. 12 can be obtained after the two groups of data are processed.

After processed preliminarily, the two groups of data need to be combined. Before the combination, they have to be registered since their "benchmarks" are different, namely that ultrasonic waves are excited at different points. Therefore, the result of directly combining the two images is incorrect definitely. Since ultrasonic waves generated by laser are transmitted in the same rail material, their speeds are the same, and accordingly, data can be registered according to the relationship between transmission speed and transmission time. The two groups of data can be converted under the same "benchmark" through calculating the difference between the total route of two exciting points and the route of any ultrasonic wave encountering defects.

The result shown as Fig. 13 can be obtained after the two groups of data are combined. According to the figure, the position of defects can be known easily, and their profiles can be obtained as well. Therefore, laser ultrasonic waves can be employed to effectively detect defects on rail surface, and solve the problem of insensitivity to defect width. In the time domain signal, a certain width of the echo signal had been received, in the process of imaging, a certain width also had been found in the contour information of the defects, therefore real contour information is hard to recognize. The extreme outer edge of the corresponding profile under the same Z value is given in the image to produce the width value of defects shown as Fig. 14, which shows that when Z is 72.5 mm, the maximum width of defects appears, namely 1.7486 mm. The error between the width and the actual maximum width 1.75 mm is 0.014%. Therefore, the imaging of defects basically reflects rail surface-connected defects, and the approach offers a new method for the effective and quantitative detection of rail defects.

4 Conclusions

To better detect rail surface-connected defects, this paper carried out the study through the approach of finite element

simulation, established the numerical model of detecting such defects through laser-excited ultrasonic waves, verified the correctness of the simulation through the experimental method, and finally discovered the results of experiment and simulation are highly identical in some parts (In the 2D simulation the geometrical spreading of the wave form is different from the 3D laser source in the rail and therefore no quantitative agreement). Since laser ultrasonic waves are insensitive to the width of defects in actual detection, the model was improved by exciting ultrasonic waves at the two sides of rail with two staggered lasers. Then, the whole profile of defects was extracted for imaging through technologies such as imaging analysis, with the error being about 0.014%. The approach offered a new method for the effective and quantitative detection of rail surface-connected defects through the laser ultrasonic wave technology.

Acknowledgements This work was supported by National Nature Science Foundation of China (Grant No. 61471304), and the authors wish to acknowledge them for their support. The authors also thank Southwest Jiaotong University NDT Research Center & Olympus NDT Joint Laboratory of Nondestructive Testing for their kind support in the experiment.

References

1. Hernandez-Valle, F., Dutton, B., Edwards, R.S.: Laser ultrasonic characterisation of branched surface-breaking defects. J. NDT & E Int. **68**, 113–119 (2014)
2. Clark, R.: Rail flaw detection: overview and needs for future developments. J. NDT & E Int. **37**(2), 111–118 (2004)
3. Palmer, S.B., Dixon, S., Edwards, R.S., Jian, X.: Transverse and longitudinal crack detection in the head of rail tracks using Rayleigh wave-like wideband guided ultrasonic waves. In: Proceedings of SPIE International Symposium on Nondestructive Evaulation for Health Monitoring & Diagnostics, vol. 5767, pp. 70–80 (2005)
4. Armitage, P.R.: The use of low-frequency Rayleigh waves to detect gauge corner cracking in railway lines. J. Insight **44**(6), 369–372 (2002)
5. Chen, Q.: Laser ultrasonic technology and its applications. J. Laser Optron. Prog. **4** (2005)
6. Yang, L., Xiang, Z.Q., Tang, Z.F.: Application of laser-induced ultrasound on rail flaw inspection. J. Mach. Des. Manuf. **10**, 26 (2009)
7. Sanderson, T., Ume, C., Jarzynski, J.: Longitudinal wave generation in laser ultrasonics. J. Ultrason. **35**(8), 553–561 (1998)
8. Rose, L.R.F.: Point-source representation for laser-generated ultrasound. J. Acoust. Soc. Am. **75**(3), 723–732 (1984)
9. Bresse, L.F., Hutchins, D.A.: Transient generation by a wide thermoelastic source at a solid surface. J. Appl. Phys. **65**(4), 1441–1446 (1989)
10. Pantano, A., Cerniglia, D.: Simulation of laser generated ultrasound with application to defect detection. J. Appl. Phys. A **91**(3), 521–528 (2008)
11. Pantano, A., Cerniglia, D.: Simulation of laser-generated ultrasonic wave propagation in solid media and air with application to NDE. J. Appl. Phys. A **98**(98), 327–336 (2010)
12. Fan, Z.H.: Computation of scattering from the complex media targets with the hybrid finite-element boundary integral method. Chin. J. Radio Sci. **24**(3), 452–456 (2009)
13. Kasai, M., Fukushima, S., Gohshi, Y., Sawada, T., Ishioka, M., Kaihara, M.: A basic analysis of pulsed photoacoustic signals using the finite elements method. J. Appl. Phys. **64**(3), 972–976 (1988)
14. Lee, J.H., Burger, C.P.: Finite element modeling of laser-generated Lamb waves. J. Comput. Struct. **54**(3), 499–514 (1995)
15. Wu, X.M., Qian, M.L.: Simulation of the finite element method on wave propagation in cylinders. In: International Workshop on Modern Acoustics-NDE, vol. 11, pp. S265–S268 (2001)
16. Hassan, W., Veronesi, W.: Finite element analysis of Rayleigh wave interaction with finite-size, surface-breaking cracks. J. Ultrason. **41**(1), 41–52 (2003)
17. Edwards, R.S., Dutton, B., Clough, A.R., Rosli, M.H.: Enhancement of ultrasonic surface waves at wedge tips and angled defects. J. Appl. Phys. Lett. **99**(9), 239 (2011)